A framework of elastic-plastic damaging model for concrete under multiaxial stress states

Loredana Contrafatto, Massimo Cuomo

A framework of elastic plastic damaging model for concrete under multiaxial stress states

L. Contrafatto *, M. Cuomo

Department of Civil and Environmental Engineering University of Catania, v.le A. Doria, 6, 95125 Catania, Italy

Abstract

The paper concerns the description and the validation of a constitutive model for concrete charac terized by a combined plastic hardening damage fracture dissipative criterion developed within the framework of the simple material model, so that its numerical implementation is easy and robust. Two different damage isotropic mechanisms associated with tensile and compressive strain processes are introduced and two hardening variables are used; the first rules the plastic hardening while the sec ond controls the compaction of the material. The limit domain is defined through the envelope of three yield criteria presenting a strong and original coupling between plastic and damage dissipative mech anisms. It is demonstrated that the proposed framework allows the reproduction of some distinctive features of the behavior of concrete under multiaxial stress states, such as volumetric hardening in tri axial compression load processes, the increment of strength under confined compression, post peak dilatancy, varying degradation of the elastic stiffness in tensile or compressive stress states, the increase of the limit strain in cyclic processes. A comparison of the numerical predictions with the literature experimental tests is presented. The limits of the proposed model are also discussed in the paper.

Keywords: B. Concrete; B. Constitutive behavior; B. Elastic plastic material; Damage mechanics

1. Introduction

The article deals with the numerical modelling of plain concrete for the 3-dimensional stress analyses requiring continuum simulations, such as those arising in dams, tunnel lin-

* Corresponding author. +39 095 738 2250; fax +39 095 738 2298.
E mail addresses: lcontra@dica.unict.it (L. Contrafatto), mcuomo@dica.unict.it (M. Cuomo).

ings, deep reservoirs, confined pillars, etc. An accurate mechanical model is especially needed in the analysis of damage, aging and degradation phenomena. Following the approaches initially suggested by Ortiz (1985), Klisinski and Mróz (1988), Pietruszczak et al. (1988), Lubliner et al. (1989), Frémond and Nedjar (1995), among others, a vast number of models have been proposed in the past decades. Most of the recent proposals include in the model plastic deformations, damage and eventually cracking strains, in an attempt to achieve reasonable accuracy in the numerical simulation of the various mechanisms of deformation and crisis that are experimentally observed.

The necessity of a model for concrete, reliable for numerical simulations, based on firm mechanical principles and, at the same time, able to reproduce significant experimental observation was first clearly identified by Ortiz (1985), whose model, based on mixture theory and damage mechanics, met most of the previously stated objectives. He made use of a Drucker Prager plasticity criterion for the aggregate and considered a prevalently brittle behavior for the mortar, yielding quite accurate qualitative predictions for simple stress states. However, more precise specification of model functions for complex load conditions was not considered.

Focussing our attention on continuum models, a variety of combination of plasticity and damage theories have been formulated. Damage is represented, according to Continuum Damage Mechanics, introducing phenomenological damage variables. Although damage is inherently a non isotropic phenomenon, in order to overcome some of the dramatic convergence problems related to the computational implementations, many authors have commonly adopted an isotropic damage formulation, making use of a single scalar variable (Luccioni et al., 1996; Jirásek and Zimmermann, 1998; Brenchic and Gambarotta, 2001; Salari et al., 2004). Scalar models with two damage variables have also been proposed, in an attempt to distinguish between tension and compression damage mechanisms (Mazars, 1986; Faria et al., 1998; Comi and Perego, 2001; Marfia et al., 2004). Following the general formulation of Hansen and Schreyer (1994) and Murakami and Kamiya (1997), anisotropic damage models have been proposed introducing 4th or more frequently 2nd order tensors (Papa and Taliercio, 1996; Dragon et al., 2000; Sellier and Bary, 2002; Litewka and Debinski, 2003; Lü et al., 2004; Kuna-Ciskał and Skrzypek, 2004; Gambarotta, 2004). However, in many of these models the flow rules for the internal variables are established on an empirical basis and are not consistently derived from a proper dissipation functional; this may lead to inconsistencies in the implementation of the model. The different crisis mechanisms of concrete are generally modelled introducing multiple limit criteria. In addition to a damage activation law, a plastic-like criterion is used in order to predict the onset of irreversible deformations. In the microplane model (Bažant et al., 1996a,b) the non-linear triaxial behavior of concrete is defined on a plane of generic orientation where the strains are projection of the macroscopic tensor; however, stress strain boundaries have to be introduced to limit the excessively large lateral strain predicted at large tensile strains and to simplify the implementation of the model originally affected by computational inefficiency. Many improvements of Bazant's initial proposal have been made (Carol et al., 2001; Bažant and Di Luzio, 2004; Park and Kim, 2005), some of which including friction phenomena (Jefferson, 2003; Gambarotta, 2004).

In spite of the huge progress made in the field, it is a common feeling that a model or a set of models generally applicable to any numerical simulations is not still available (e.g. Jefferson, 2003). The purpose of the paper is not to propose a new general model able to simulate all the mechanical behaviors of concrete; rather it aims to give methodological

contributions that can help to overcome some of the above described difficulties. The primary concern is the necessity of a reliable and efficient implementation of the model in traditional numerical codes, even for rather complex boundary value problems. Recently, a newly derived globally convergent algorithm has been proposed, specifically developed for coupled multiple criteria models such as those characteristic for concrete (Contrafatto and Cuomo, 2005). Robust algorithms are obtained if the framework of generalized simple material is preserved (Germain, 1973; Halphen and Nguyen, 1975). Setting this as a starting point, thermodynamic requirements are easily met. It is observed, to this purpose, that plasticity criteria based on effective stresses may not, in general, be compatible with the framework of simple materials (Contrafatto and Cuomo, 2002).

The paper adopts a continuum phenomenological approach involving mechanical damage and applies the methodology introduced in Contrafatto and Cuomo (2002). Thanks to its strong thermodynamical foundation it can be extended to non-mechanical (chemical) interactions. It assumes cohesive fracture and describes the progressive degradation of the elastic and hardening properties by means of the introduction of internal damaging variables. To reproduce the distinctive different behavior in tension and compression a generalization of Curnier's bi-modular materials (Curnier et al., 1993) is proposed for the internal energy and the dissipation functional, obtained through the split of a damage coupled free energy between tensile and compressive states. Fully coupled damage and plasticity multiple crisis criteria are used in order to predict the difference between elastic and peak limit states without introducing a preassigned saturation domain; a continuous transition from hardening to softening is so obtained, which depends on the load history. The damage evolution affects the elastic stiffness and the strength of the material as well. Several phenomena are modelled, such as the non-linearity of the stress strain curve, the post-peak dilatancy, the cyclic behavior, including the dependence of the peak stress on the previous history, the progressive increment of the limit strain under cyclic tests, etc.; strength increment under confined compression and volumetric hardening under triaxial compression are also detected. Since the model is based on firm thermodynamic principles, i.e. energy transfer functionals are defined, it is possible to simulate the behavior of different types of concrete, including high performance concrete, by simply choosing the correct values for the model parameters and so moving from a "ductile" to a brittle behavior.

The two energy functionals ruling the model depend on few material parameters, to which can be given mechanical meanings. In this sense the energy functionals adopted are not based on interpolation data. It must be pointed out that it is very hard to obtain a precise estimation of the material parameters for a strongly coupled model like the one presented. Procedures based on numerical algorithms are often used to this end (Bažant et al., 1996b; Bolzon et al., 2002). The parameter determination procedure illustrated in the paper is a simplified one, but it allows approximated values of the constitutive parameters for preliminary analyses to be obtained. More accurate instruments, based for instance on genetic algorithms, would be required.

In the paper specific forms of internal energy, of dissipation functional and of damage measures are assumed. This does not mean that they are applicable in all cases, since, given the diversity of phenomena that must be modelled, and the ever increasing findings of research, better and more realistic forms can surely be suggested, possibly problem-oriented. Our aim is to show how, even when making rather simplified hypotheses, the adopted framework is able to reproduce many experiments, without introducing ad hoc assumptions. The authors are perfectly aware of a number of limitations still present in

the current form of the model. The most important is that an accurate description of damage would require anisotropic internal variables. In that case the general form of the internal energy is well known and derives from the theory of structural tensors (Papadopulos and Lü, 2001). A complete development of the equations for the anisotropic damage will be presented in a subsequent paper. However, since scalar damage, as observed by many authors even recently, is often sufficient to describe the response of concrete elements, unless rapidly rotating stress states are present, scalar damage variables are used here in order to simplify the treatment. It is underlined that, thanks to the introduction of different damage mechanisms associated to tensile and compressive strain processes, the model is quasi-isotropic; as a consequence rotating cracks are predicted, at least for load path which does not undergo substantial variation. The use of scalar damage is also strongly motivated by the lack of reliable data on the damage evolution of concrete under rather complex stress states. In addition, the lack of extensive experimental results for nearly isotropic compression states has been the cause of a very rough choice for the dissipation functional ruling these stress states. A further limitation is the development of the model in a time-independent frame, the time dependency having been considered only for the plastic-damage behavior.

In this paper, the constitutive model is described but all the problems related with the onset of strain localization are not considered. Applications to some structural problems will be presented in a subsequent paper, where numerical strategies for the solution of the non-linear problem and for avoiding mesh-dependency of the solution will be illustrated as well.

In the following section some considerations about the experimental behaviour of concrete and its crisis mechanisms are reported. In Section 3, the model is presented in detail. Specifically, Section 3.2 concerns the reversible behavior and Section 3.3 the irreversible behavior. The predictions for some limit states will be discussed in Section 4, where the identification of the constitutive parameters is treated too. In Section 5, the prediction of the model under multiaxial stress states is discussed and compared with experimental results. Some conclusions close the paper.

2. Experimental behavior of concrete under multiaxial stress states

The main experimental observation that the model attempts to reproduce is the lack of a clearly defined elastic response except for very small deformations; actually, damage and cracks form and develop from very low values of the load, well before the peak stress is attained. In uniaxial compression tests the level at which cracks start to propagate is roughly equal to 30% of the peak stress. Damage evolution needs then to be included in any phenomenological model, together with, however, some plastic dissipation mode, since it is known that beyond a certain deformation level permanent deformations arise in the material. This is due to crushing or the collapse of microvoids. Moreover, crack patterns in tension and compression appear quite different, both in their orientations and mechanisms (cracks in compression have greater tangential relative displacements). Different damage mechanisms in the tension and compression ranges are then introduced.

One major problem in constructing a full triaxial model for concrete is that many experimental observations apply to uniaxial behavior, and indeed a variety of models, empirically founded, exists for the uniaxial response, that are of great utility in the practical analysis of frame members. The multiaxial case is still a matter of investigation, and very

few systematic experimental observations exist that can throw some light on basic aspects of the non-linear response of concrete: among these, loading unloading behavior and careful detection of the decay of the elastic stiffness, correlation between damage and stress state, possibly using non-destructive techniques, iso-damage envelopes, measures of ductility for triaxial stress states, etc. However, some investigations have been carried out for finding the envelopes of the peak stress under bi- and tri-axial stress states, although very little information exists for stress states close to the hydrostatic compression axis. After the classical experiments of Kupfer and Gerstle (1973), extensive but, unfortunately, not exhaustive data have recently been furnished for instance by Mier (1984) and Sfer et al. (2002). The crisis modes have also been analyzed, identifying the crack patterns that form at the collapse point for different ranges of stress states, under biaxial and triaxial stress states (Mier, 1984). While cracks are nearly orthogonal to the maximum principal stress in tensile tests, in stress states characterized by predominant compression diagonal shear cracks form at failure. In triaxial compression two main collapse mechanisms have been observed. One, characterized by the formation of few large cracks, is typical of stress states obtained by superimposing an uniaxial tension on a hydrostatic compression state (stress states lying close to the tension meridian). The other, characterized by the formation of many small cracks, is typical of stress states obtained superimposing an uniaxial compression on a hydrostatic compression state (stress states lying close to the compression meridian). Isotropic compression tests reveal a sharp hardening branch, due to the compaction of the material thanks to void closure (see Fig. 11(a) for an exemplification).

3. A constitutive framework for plain concrete

Aim of the next sections is to show how some of the most significant characteristic properties of concrete behavior can be adequately reproduced within the mechanics of simple materials (Germain, 1973; Halphen and Nguyen, 1975) by simply defining appropriate internal energy and dissipation functionals, provided they are formulated in a fully coupled way in the extended space of the internal variables, according to the general plastic-hardening-damage model illustrated in Contrafatto and Cuomo (2002). The model that will be derived, thus, does not make use of ad hoc rules for catching peculiar aspects of the mechanical response. In the authors' minds any improvement to the model should be formulated directly in terms of a redefinition of the energy functionals ruling the problem. This allows a much more robust numerical implementation of the model, that is one of the main concerns for practical applications. The model, in this way, does not make a strong distinction between plasticity and damage, that are thoroughly coupled, in principle, in any yield function used. It is the form of these functions, and the type of the internal variables that occur in them that give rise to a plastic-like behavior such as the one in prevailing compression states, or to a brittle-like behavior.

Damage and hardening internal variables are used to obtain the goal described above. Hardening internal variables are introduced in connection with compression stress states, when ductility is observed, to model the fact that after the limit elastic state, well below the peak stress, stresses grow substantially but at the expense of permanent deformations. In this way, the stress strain curve, even in the pre-peak range, is not linear. Unloading, however, is linear, given the standard plastic nature of the model. Damage variables are responsible for phenomenologically reproducing the strength and the stiffness reduction: two different damage mechanisms associated with tensile and compressive strain processes

are enclosed, related to two different scalar damage variables. The use of two damage variables is essential in modelling the jump in the tangent stiffness, experimentally observed in load reversed tests. Moreover, as observed in Section 2, the direction of the microcracks are essentially different whether a compressive or a tensile stress state is applied. The two damage mechanisms lead to a bimodular material, extending the proposal of Curnier et al. (1993) to a damaging material. Of course, much more complex damage patterns dependent on the stress states are observed, and a directional description of damage is in general required. The limitation to the two scalar measures of damage adopted in the present paper restricts the use of the model to processes where the load path does not change dramatically during the stress history.

In the following section the generalized constitutive equations are introduced, starting from the state variables. In Section 3.2, the internal energy potential is defined and specifically in Sections 3.2.1 and 3.2.2, the elastic and hardening potentials are, respectively introduced. In Section 3.2.3 the form of the generalised elastic relations is given in detail. Section 3.3 concerns the inelastic behavior of the material: the dissipation functional is defined in Section 3.3.1 and, finally, in Section 3.3.2 the generalized elastic domain is specified.

3.1. Field variables and generalized elastic constitutive equations

The model is characterized by the following kinematic and dual static variables:

$\varepsilon \in \mathscr{D}$ macroscopic strain;
$\alpha \in R$ isotropic hardening;
$\alpha^v \in R$ volumetric hardening;
$\omega_1 \in R$ tensile damage;
$\omega_2 \in R$ compressive damage;
$\sigma \in \mathscr{D}$ stress;
$\chi \in R$ hardening internal forces;
$\chi^v \in R$ volumetric hardening internal forces;
$\zeta_1 \in R$ tensile damage driving forces;
$\zeta_2 \in R$ compressive damage driving forces

where $\mathscr{D}$ being the space of the second-order symmetric tensors.

It is important to underline that the deformations are regular functions throughout the whole structural domain. Note also that the internal variables are all scalar functions. Indeed kinematic hardening is not considered important for concrete. Also the damage variables are considered as scalars: this is an obvious limitation, since for an accurate description of damage the internal variables should be of tensorial nature, in order to keep track of the planes of fracture (Mosler and Bruhns, 2004). Furthermore, damage affects the elastic moduli for tensile or compressive stress states differently, since a discontinuity is observable in loading–unloading stress paths. Only the latter property is included in the analysis, adopting two different scalar damage variables associated with tensile and compressive strain processes. Following traditional arguments, both damage variables are assumed ranging into $[-1,0]$.

The internal virtual power for an isothermal process is then:

$$P_{\mathrm{vi}} = \langle \sigma, \dot{\varepsilon} \rangle + \langle \chi, \dot{\alpha} \rangle + \langle \chi^{\mathrm{v}}, \dot{\alpha}^{\mathrm{v}} \rangle + \langle \zeta_1, \dot{\omega}_1 \rangle + \langle \zeta_2, \dot{\omega}_2 \rangle \tag{1}$$

In (1) the power of the hardening and damage variables is equal to zero. That is the dimension of the reference volume to which the model applies is large enough so that the energy flux through its boundaries is due only to the mechanical work of the stresses. Therefore, the total value of the internal variables α, α^{v}, ω_1, ω_2 is set equal to zero.

The model is implemented in the hypothesis of small deformations and each kinematic variable is additively decomposed in a reversible and an irreversible component, in a classic way:

$$\varepsilon = \varepsilon_e + \varepsilon_p \begin{cases} \alpha = \alpha_e + \alpha_p = 0 \\ \alpha^{v} = \alpha_e^{v} + \alpha_p^{v} = 0 \end{cases} \begin{cases} \omega_1 = \omega_{1_e} + \omega_{1_p} = 0 \\ \omega_2 = \omega_{2_e} + \omega_{2_p} = 0 \end{cases}$$

With compact notation the state of the system is described by the two sets of dual kinematic and static state variables η and τ:

$$\eta = (\varepsilon,\alpha,\alpha^{v},\omega_1,\omega_2) = \eta_e + \eta_p, \quad \tau = (\sigma,\chi,\chi^{v},\zeta_1,\zeta_2)$$

Since the evolution of the mechanical properties of concrete depends on physically well defined dissipation mechanisms, the main effort of the present model is to define all the evolution mechanisms in an energetic way, postulating the existence of two functionals, one of the internal energy $e(\eta_e)$ and the other of dissipation $d(\dot{\eta}_p)$. Thus concrete is considered as a simple material, as in the definition of Germain (1973). The apparently redundant distinction between reversible and irreversible components of the internal damage variables (i.e. $\omega_e \quad -\omega_p$), is mainly motivated by the intention of distinguishing the kinematic variables that are responsible for storage energy and for dissipation, as stated in Contrafatto and Cuomo (2002).

By standard thermodynamic arguments the driving forces τ, dual to the kinematic variables η_e, are obtained differentiating the free energy

$$\tau \in \partial_{\eta_e} e(\eta_e)$$

where the symbol ∂ denotes sub-differentiation, in order to account for the common case of non-smooth energy functionals. Conjugated potentials $e^{c}(\tau)$ and $d^{c}(\tau)$ are derivable through a Fenchel transformation; moreover, the following conditions hold:

$$\begin{aligned} &e^{c}(\tau) + e(\eta_e) = \langle \tau,\eta_e \rangle \\ &d^{c}(\tau) + d(\dot{\eta}_e) = \langle \tau,\dot{\eta}_p \rangle \end{aligned} \iff \begin{aligned} &\tau \in \partial_{\eta_e} e(\eta_e), \quad \eta_e \in \partial_{\tau} e^{c}(\tau) \\ &\tau \in \partial_{\eta_p} d(\dot{\eta}_p), \quad \dot{\eta}_p \in \partial_{\tau} d^{c}(\tau) \end{aligned} \tag{2}$$

Constitutive conditions, then, can be specified assigning either the energy potentials or their conjugated.

3.2. Internal stored energy potential

The stored energy, function of the reversible components of all the kinematic variables, is given by the sum of the elastic deformation energy $\phi(\varepsilon_e,\omega_{1_e},\omega_{2_e})$ and of the hardening (configuration) energy $\psi_1(\alpha_e,\omega_{1_e},\omega_{2_e}) + \psi_2(\alpha_e^{v})$, both coupled with damage:

$$\begin{aligned} &e(\varepsilon_e,\alpha_e,\alpha_e^{v},\omega_{1_e},\omega_{2_e}) = \phi(\varepsilon_e,\omega_{1_e},\omega_{2_e}) + \psi_1(\alpha_e,\omega_{1_e},\omega_{2_e}) + \psi_2(\alpha_e^{v}) + \operatorname{ind} W_1(\omega_{1_e}) + \operatorname{ind} W_2(\omega_{2_e}) \\ &W_1 = \{\omega_{1_e} : -1 \leqslant \omega_{1_e} \leqslant 0\} \quad W_2 = \{\omega_{2_e} : -1 \leqslant \omega_{2_e} \leqslant 0\} \\ &\operatorname{ind} W(\omega_e) = \begin{cases} 0 & \text{if} \quad \omega_e \in W \\ +\infty & \text{if} \quad \omega_e \notin W \end{cases} \end{aligned} \tag{3}$$

where the last two terms enforce the admissibility constraints for the damage variables. The elastic relations are obtained from the variation of e w.r.t the kinematic variables:

$$\sigma = \partial_{\varepsilon_e}\phi \quad \zeta_1 = \partial_{\omega_{1_e}}\phi + \partial_{\omega_{1_e}}\psi_1 + \zeta_{1_a} \quad \zeta_{1_a} \in \partial \mathrm{ind}\, W_1(\omega_{1_e})$$
$$\chi = \partial_{\alpha_e}\psi_1 \quad \zeta_2 = \partial_{\omega_{2_e}}\phi + \partial_{\omega_{2_e}}\psi_1 + \zeta_{2_a} \quad \zeta_{2_a} \in \partial \mathrm{ind}\, W_2(\omega_{2_e})$$
$$\chi^v = \partial_{\alpha_e^v}\psi_2$$

3.2.1. Elastic energy potential

A general methodology for bimodular elastic materials was introduced by Curnier et al. (1993). It consists in subdividing the strain space into a compression domain $\mathscr{D}^-$ and a tension domain $\mathscr{D}^+$, separated by hypersurfaces (separating interfaces) defined through functions of the strain invariants. The original proposal of Curnier has been extended to a generalized kinematic space that contains, in addition to the elastic strains, the damage internal variables.

The continuity of the stress strain law requires the respect of the following properties:

- the separating interface $z(\varepsilon_e)$ must contain the origin of the strain space;
- the positive and negative subdomains $\mathscr{D}^+$ and $\mathscr{D}^-$ must be simply connected;
- the elastic energy must be continuous across the interface

$$\phi(\varepsilon_e,\omega_{1_e},\omega_{2_e}) = \phi^+(\varepsilon_e,\omega_{1_e},\omega_{2_e}) = \phi^-(\varepsilon_e,\omega_{1_e},\omega_{2_e}) \quad \forall \varepsilon_e : z(\varepsilon_e) = 0$$

- the gradient of the elastic energy must be continuous across the interface (continuity of the stress strain law)

$$\nabla_{\varepsilon_e}\phi^+ = \nabla_{\varepsilon_e}\phi^- \Rightarrow \sigma^+(\varepsilon_e,\omega_{1_e},\omega_{2_e}) = \sigma^-(\varepsilon_e,\omega_{1_e},\omega_{2_e}) \quad \forall \varepsilon_e : z(\varepsilon_e) = 0$$

- the jump in the hessian of the elastic energy (elastic tensor) across the interface must be normal to the interface

$$\nabla_{\varepsilon_e}\sigma^+ - \nabla_{\varepsilon_e}\sigma^- = s(\varepsilon_e)\nabla_{\varepsilon_e}z(\varepsilon_e) \otimes \nabla_{\varepsilon_e}z(\varepsilon_e) \quad \forall \varepsilon_e : z(\varepsilon_e) = 0$$

in which $s(\varepsilon_e)$ is a scalar function of the strain state.

Different proposals for the separating interface are possible. The authors, in a preliminary work (Contrafatto and Cuomo, 2000), have examined two of them. The simplest choice directly derived by the original Curnier proposal, is to take, as separating interface, the deviatoric plane $\mathrm{tr}\,\varepsilon_e \quad 0$ in the space of the elastic strain. The deviatoric plane $\mathrm{tr}\,\varepsilon_e \quad 0$ so that the elastic energy takes different forms according to the sign of the trace of the elastic strain tensor. The choice commonly assumed when a bimodular material model is adopted (Comi and Perego, 2001; Faria et al., 1998) is coupled with an isotropic damage model. As an alternative choice, the separating interface can be defined by the eigenvalues of the elastic strain tensor, often splitting it into its tensile and compressive components by means of a polar decomposition (Lubarda et al., 1994; Papa and Taliercio, 1996; Carlson and Hoger, 1986). The last choice seems more appropriate for a non-isotropic damage model. In the following the interface $\mathrm{tr}\,\varepsilon_e \quad 0$ is adopted, that is sufficient for illustrating the potentiality of the constitutive framework proposed. It is important to underline that in both the expressions $\phi \quad$ and ϕ^+ of the elastic energy appears either the tensile damage ω_{1_e} and the compressive damage ω_{2_e} and that the difference between their expressions relies in their functional dependence on these variables.

The following definition of the elastic energy has then been adopted

$$\Phi = \begin{cases} \Phi^+(\varepsilon_e,\omega_{1_e},\omega_{2_e}) = \frac{1}{2}\left[2G^+\varepsilon_e\cdot\varepsilon_e + \lambda^+ \mathrm{tr}^2\varepsilon_e\right] & \text{if} \quad \mathrm{tr}\,\varepsilon_e \geqslant 0 \\ \Phi^-(\varepsilon_e,\omega_{1_e},\omega_{2_e}) = \frac{1}{2}\left[2G^-\varepsilon_e\cdot\varepsilon_e + \lambda^- \mathrm{tr}^2\varepsilon_e\right] & \text{if} \quad \mathrm{tr}\,\varepsilon_e \leqslant 0 \end{cases} \tag{4}$$

where G^+, G , λ^+, λ are the generalized Lame coefficients, all depending on the pair $(\omega_{1_e},\omega_{2_e})$.

The continuity and jump conditions across the interface $\mathrm{tr}\,\varepsilon_e$ 0 take the form:

$$2G^+\varepsilon_e = 2G^-\varepsilon_e$$
$$\nabla\sigma^+ - \nabla\sigma^- = s(\varepsilon_e)(\lambda^+ - \lambda^-)I\otimes I$$

The first of these conditions implies that the shear modulus is constant across the interface $\mathrm{tr}\,\varepsilon_e$ 0, i.e. $G^+(\omega_{1_e},\omega_{2_e}) = G^-(\omega_{1_e},\omega_{2_e})$, so that only three parameters can be assigned independently. The following choice for the elastic moduli has been made:

$$\begin{aligned} G^+(\omega_{1_e},\omega_{2_e}) &= G^-(\omega_{1_e},\omega_{2_e}) = G(\omega_{1_e},\omega_{2_e}) = G_0(1+\omega_{1_e})^{n_1}(1+\omega_{2_e})^{n_2} \\ \lambda^+(\omega_{1_e},\omega_{2_e}) &= \left[K_0 - \frac{2}{3}G_0(1+\omega_{2_e})^{n_2}\right](1+\omega_{1_e})^{n_1} \\ \lambda^-(\omega_{1_e},\omega_{2_e}) &= K_0 - \frac{2}{3}G_0(1+\omega_{1_e})^{n_1}(1+\omega_{2_e})^{n_2}(1+\omega_{1_e})^{n_1} \end{aligned} \tag{5}$$

G_0 and K_0 being the undamaged elastic constants. The choice is motivated by experimental evidence: in fact, the bulk modulus K_0 $(2G_0 + 3\lambda_0)/3$ remains undamaged in compression, while on radial paths in traction a progressive loss of stiffness in the deviatoric space is observed.

3.2.2. Hardening potentials

The hardening potential in (3) is given by the sum of two contributions. The first rules the evolution of the elastic domain:

$$\Psi_1(\alpha_e,\omega_{1_e},\omega_{2_e}) = \frac{1}{2}H[p_1(1+\omega_{1_e})^{n_1} + p_2(1+\omega_{2_e})^{n_2}]\alpha_e^2 \quad p_1+p_2 = 1 \tag{6}$$

In (6) p_1 and p_2 are weight scalars setting the influence degree of tensile and compressive damage on hardening. The underlying assumption for the hardening potential (6) is that, after a rather low level of stress, irreversible phenomena such as microcracks occur, causing irreversible strains as well as a decay of the tangent stiffness. Thanks to the structure of formula (6) it is possible to model the non linear ascending branch of the stress strain behavior of concrete, without introducing ad hoc rules. Moreover, the onset of damage, observed well before the peak stress is reached, is correctly reproduced.

The second term in (3) is the volumetric hardening potential, accounting for the recovery of stiffness following initial degradation when concrete is loaded along the hydrostatic compression axis. According to experimental observations (see Section 4) it has been defined as (Resende, 1987)

$$\Psi_2(\alpha_e^v) = D\frac{a-\alpha_e^v}{a}\left[\ln\frac{a-\alpha_e^v}{a} - 1\right] \tag{7}$$

where a is the maximum degree of compaction and D has the dimension of an elastic stiffness and it will be better qualified in Section 4.3. The dimensionless ratio $\frac{a-\alpha_e^v}{a}$ ranges between 0 and 1.

3.2.3. Generalized elastic relations

From definitions (4) (7) the expression of the generalized elastic relations follows:

$$
\begin{aligned}
&\sigma = \begin{cases} \sigma^{+} = 2G\varepsilon_{\mathrm{e}} + \lambda^{+}\mathrm{tr}\,\varepsilon_{\mathrm{e}} & \mathrm{tr}\,\varepsilon_{\mathrm{e}} \geqslant 0 \\ \sigma^{-} = 2G\varepsilon_{\mathrm{e}} + \lambda^{-}\mathrm{tr}\,\varepsilon_{\mathrm{e}} & \mathrm{tr}\,\varepsilon_{\mathrm{e}} \leqslant 0 \end{cases} \\
&\chi = Hf(\omega_{1_{\mathrm{e}}},\omega_{2_{\mathrm{e}}})\alpha_{\mathrm{e}} \\
&\chi^{\mathrm{v}} = \frac{D}{a}\ln\left(\frac{a}{a-\alpha_{\mathrm{e}}^{\mathrm{v}}}\right) \\
&\zeta_1 = \begin{cases} \zeta_1^{+} = \frac{1}{2}\left[2\frac{\partial G}{\partial\omega_{1_{\mathrm{e}}}}\varepsilon_{\mathrm{e}}\cdot\varepsilon_{\mathrm{e}} + \frac{\partial\lambda^{+}}{\partial\omega_{1_{\mathrm{e}}}}\mathrm{tr}^2\varepsilon_{\mathrm{e}}\right] + \frac{1}{2}H\alpha_{\mathrm{e}}^2\frac{\partial f}{\partial\omega_{1_{\mathrm{e}}}} + \zeta_{1_a} & \mathrm{tr}\,\varepsilon_{\mathrm{e}} \geqslant 0 \\ \zeta_1^{-} = \frac{1}{2}\left[2\frac{\partial G}{\partial\omega_{1_{\mathrm{e}}}}\varepsilon_{\mathrm{e}}\cdot\varepsilon_{\mathrm{e}} + \frac{\partial\lambda}{\partial\omega_{1_{\mathrm{e}}}}\mathrm{tr}^2\varepsilon_{\mathrm{e}}\right] + \frac{1}{2}H\alpha_{\mathrm{e}}^2\frac{\partial f}{\partial\omega_{1_{\mathrm{e}}}} + \zeta_{1_a} & \mathrm{tr}\,\varepsilon_{\mathrm{e}} \leqslant 0 \end{cases} \\
&\zeta_2 = \zeta_2^{+} = \zeta_2^{-} = \frac{1}{2}\left[2\frac{\partial G}{\partial\omega_{2_{\mathrm{e}}}}\varepsilon_{\mathrm{e}}\cdot\varepsilon_{\mathrm{e}} + \frac{\partial\lambda^{+}}{\partial\omega_{2_{\mathrm{e}}}}\mathrm{tr}^2\varepsilon_{\mathrm{e}}\right] + \frac{1}{2}H\alpha_{\mathrm{e}}^2\frac{\partial f}{\partial\omega_{2_{\mathrm{e}}}} + \zeta_{2_a}
\end{aligned}
\tag{8}
$$

$$
\begin{aligned}
&f(\omega_{1_{\mathrm{e}}},\omega_{2_{\mathrm{e}}}) = p_1(1+\omega_{1_{\mathrm{e}}})^{n_1} + p_2(1+\omega_{2_{\mathrm{e}}})^{n_2} \\
&\frac{\partial f}{\partial\omega_{1_{\mathrm{e}}}} = n_1p_1(1+\omega_{1_{\mathrm{e}}})^{n_1-1} \qquad \frac{\partial f}{\partial\omega_{2_{\mathrm{e}}}} = n_2p_2(1+\omega_{2_{\mathrm{e}}})^{n_2-1} \\
&\frac{\partial G}{\partial\omega_{1_{\mathrm{e}}}} = n_1G_0(1+\omega_{1_{\mathrm{e}}})^{n_1-1}(1+\omega_{2_{\mathrm{e}}})^{n_2} \\
&\frac{\partial G}{\partial\omega_{2_{\mathrm{e}}}} = n_2G_0(1+\omega_{1_{\mathrm{e}}})^{n_1}(1+\omega_{2_{\mathrm{e}}})^{n_2-1} \\
&\frac{\partial\lambda^{+}}{\partial\omega_{1_{\mathrm{e}}}} = n_1\left[K_0 - \frac{2}{3}G_0(1+\omega_{2_{\mathrm{e}}})^{n_2}\right](1+\omega_{1_{\mathrm{e}}})^{n_1-1} \\
&\frac{\partial\lambda^{-}}{\partial\omega_{1_{\mathrm{e}}}} = K_0 - \frac{2}{3}n_1G_0(1+\omega_{1_{\mathrm{e}}})^{n_1-1}(1+\omega_{2_{\mathrm{e}}})^{n_2} \\
&\frac{\partial\lambda^{+}}{\partial\omega_{2_{\mathrm{e}}}} = \frac{\partial\lambda^{-}}{\partial\omega_{2_{\mathrm{e}}}} = -\frac{2}{3}n_2G_0(1+\omega_{1_{\mathrm{e}}})^{n_1}(1+\omega_{2_{\mathrm{e}}})^{n_2-1}
\end{aligned}
$$

Therefore, a different development for the tensile damage driving force ζ_1 is obtained according to whether a strain process with positive or negative trace is considered (and in any case with trace different from zero). The compressive damage force ζ_2 develops, on the contrary, in the same way in both subdomains.

3.3. The inelastic behavior

3.3.1. The dissipation functional

As stated after Eq. (2), constitutive equations for the inelastic behavior are specified assigning the conjugate dissipation potential. The dual (complementary) potential proposed is the indicator function of a suitable generalized elastic domain

$$
d^{c}(\tau) = \mathrm{ind}K(\tau) \quad K(\tau) = \{\tau : g(\tau) \leqslant 0\} \tag{9}
$$

$g(\tau)$ being the yield function. Therefore the dissipation is uniquely defined once a form for the yield function is chosen. From (2) the flow rule for the inelastic variables follows:

$$
\dot{\eta}_{\mathrm{p}} \in \lambda\partial_{\tau}g(\tau) \tag{10}
$$

A strain rate dependent behavior is also considered for processes whose time scale is comparable with a characteristic relaxation time of the material. In this paper the case of a long relaxation time is considered, characterizing irreversible phenomena such as plasticity and damage. The model so obtained is a generalized viscoplastic one, including a Perzyna-type formulation for the strain rate

$$\dot{\eta}_{\mathrm{p}} = \mu \left[\frac{g(\tau)}{\tau_0} \right]_+ \partial g(\tau) \tag{11}$$

the bracket being the overstress function. In (11), $g(\tau)$ is the yield function defined in (9) and τ_0 is a parameter indicating the original radius of the elastic domain.

3.3.2. Generalized elastic domain

The generalized elastic domain K is defined in the extended space of stresses, thermodynamic forces and conjugated damage variables. It is assumed as the convex hull of three crisis surfaces:

$$\begin{aligned} & & g_1(\sigma,\chi,\zeta_2) &= f(I_1,J_2,J_3,\chi,\zeta_2) \\ g(\tau) = \max\{g_1,g_2,g_3\} \quad & g_2(\sigma,\zeta_1) & &= \alpha I_1(\sigma) + \beta\sqrt{J_2(\sigma)} + \zeta_1 - \zeta_0 \\ & g_3(\sigma,\chi^{\mathrm{v}}) & &= -\sigma_{\mathrm{m}} + \sigma_{\mathrm{m}}^{\mathrm{c}} - \chi^{\mathrm{v}} \end{aligned}$$

$$I_1 = \operatorname{tr}\sigma, \quad J_2 = \frac{1}{2}\operatorname{dev}\sigma \cdot \operatorname{dev}\sigma, \quad J_3 = \det \operatorname{dev}\sigma \quad \zeta_0, \quad \sigma_{\mathrm{m}}^{c} \in R \quad \sigma_{\mathrm{m}} = \frac{1}{3} I_1$$

The function g_1 is a plastic yield criterion, able to model the behavior of concrete in the range of triaxial compression with low lateral confinement; the introduction of the isotropic hardening variable χ and of the static damage variable ζ_2 causes the initial expansion, followed by the contraction of the domain when damage in compression is active. An extended Ottosen criterion has been adopted:

$$g_1(\sigma,\chi,\zeta_2) = b_1 I_1(\sigma) + \frac{b_2}{f_{\mathrm{c}}^{\star}} J_2(\sigma) + \lambda(\cos 3\theta(\sigma))\sqrt{J_2(\sigma)} - f_{\mathrm{c}}^{\star}$$

$$b_1,b_2,f_{\mathrm{c}}^{\star} \in R^+ \quad \cos 3\theta(\sigma) = \frac{3}{2}\frac{\sqrt{3J_3(\sigma)}}{J_2(\sigma)\sqrt{J_2(\sigma)}}$$

$$\lambda(\cos 3\theta(\sigma)) = \begin{cases} k_1 \cos\left[\frac{1}{3}\arccos(k_2 \cos 3\theta(\sigma))\right], & \cos 3\theta \geqslant 0, \quad k_1 > 0 \\ k_1 \cos\left[\pi - \frac{1}{3}\arccos(-k_2 \cos 3\theta(\sigma))\right], & \cos 3\theta < 0, \quad 0 \leqslant k_2 < 1 \end{cases}$$

$\theta(\sigma)$ being the Lode angle and b_1, b_2, k_1, k_2 material constants defining the amplitude and the shape of the deviatoric sections. The compressive strength $f_{\mathrm{c}}^{\star}$ is a function of the compression elastic limit f_{c}, of the hardening χ and of damage ζ_2, in the form:

$$f_{\mathrm{c}}^{\star} = f_{\mathrm{c}} + \chi - k_{\zeta}\zeta$$

the parameter k_{ζ} representing an adjustable damage rate.

The hardening and damage variables evolve according to the elastic constitutive equations. When a proportional loading is applied, the static variables (σ, χ, ζ_2) follow a complex path in the generalized stress space; the Ottosen limit state is obtained when this path intersects the limit surface g_1. Therefore, the elastic domain is rather different from the classical one proposed by Ottosen (1977) and it depends also on the form

chosen for the internal energy, that links the evolution of the damage energy to the stress state.

In the same way, the elastic limit state changes with the damage coefficient n_2, that is, it can also be influenced by environmental factors affecting the damage rate. The peak domain, on the contrary, can only be evaluated numerically, and it depends, consequently, on the particular load path followed. This aspect will be discussed in Section 4.

The function g_2 is a damage-like criterion for tensile stresses. The limit ζ_0 is related to the fracture energy, as will be better examined in Section 4.1. Moreover, the criterion is coupled with the first and the second stress invariant, so that permanent deformations are found upon unloading.

The function g_3 represents a volumetric cap along the hydrostatic axis translating with the hardening conjugated variable χ^{v}. Introducing the constitutive equation for χ_{v} it can be observed that the cap moves toward infinity as the compaction degree grows. The expression of this yield function is quite primitive since experimental information is insufficient. Coupling with the deviatoric part of the stress tensor, in a way similar to the elliptic cap model (DiMaggio and Sandler, 1971), would be required for the transition regime.

4. Predictions of the model for simple loading histories and parameters estimate

The model presented in Section 3 is characterized by a fair number of material parameters. Namely,

- *Internal energy*:
  initial elastic moduli G_0 and λ_0 (or initial Young modulus E_0 and Poisson's ratio v_0);
  initial hardening modulus H_0;
  damage rate exponents n_1 and n_2.
- *Ottosen-like criterion*:
  b_1, b_2, k_1, k_2 coefficients;
  uniaxial elastic limit stress in compression f_{c};
  damage rate k_ζ.
- *Fracture criterion*:
  energy of fracture propagation ζ_0;
  α, β coefficients.
- *Hydrostatic cap*:
  maximum degree of compaction a;
  compaction rate D;
  limit elastic hydrostatic stress $\sigma_{\mathrm{m}}^{\mathrm{c}}$.

Not all of them can be easily correlated to a single material property. In this section we will examine some simple loading histories, in order to highlight the performance of the model and the physical meaning of the parameters. The model has been calibrated and compared to classical experimental data available in the literature. However, the effect of the parameters on the predictions of the model is deeply coupled and, given a limited set of experimental results, usually identification procedures should be adopted.

Few experimental campaigns on concrete behavior under multiaxial stress states are available. In this work Van Mier data, concerning uniaxial, biaxial and triaxial states of stress, have been used especially for parameter calibration, as they include the results of cyclic tests that allow the estimation of the linear elastic limit stress with some accuracy and give information about the damaged unloading behavior (Mier, 1984).

For the numerical simulation the constitutive model has been implemented in the FEAP code (Taylor, 2002).

4.1. Tensile processes

For uniaxial tensile process the constitutive relations state that:

$$\begin{aligned}
\sigma_1 &= \frac{9G_0K_0(1+\omega_{1_e})^{n_1}(1+\omega_{2_e})^{n_2}}{3K_0+G_0(1+\omega_{2_e})^{n_2}}\varepsilon_{e_1} \\
\zeta_1 &= \frac{n_1}{2}\frac{9G_0K_0(1+\omega_{1_e})^{n_1-1}(1+\omega_{2_e})^{n_2}}{3K_0+G_0(1+\omega_{2_e})^{n_2}}\varepsilon_{e_1}^2 \\
\zeta_2 &= \frac{n_2}{2}\frac{27G_0K_0^2(1+\omega_{1_e})^{n_1}(1+\omega_{2_e})^{n_2-1}}{[3K_0+G_0(1+\omega_{2_e})^{n_2}]^2}\varepsilon_{e_1}^2 \\
\nu^+ &= \frac{3K_0-2G_0(1+\omega_{2_e})^{n_2}}{2[3K_0+G_0(1+\omega_{2_e})^{n_2}]}
\end{aligned} \tag{12}$$

Note that both the damage static variables ζ_1 and ζ_2 are different from zero even in the elastic range when $\omega_{1_e} = \omega_{2_e} = 0$. They develop during the entire elastic loading process.

The tensile limit stress is obtained enforcing the condition $g_2 \quad 0$ in the uniaxial state:

$$\sigma_1' = \frac{E_0}{n_1}\left(\alpha+\frac{\beta}{\sqrt{3}}\right)\left[\sqrt{1+\frac{2n_1}{E_0}\frac{\zeta_0}{\left(\alpha+\frac{\beta}{\sqrt{3}}\right)^2}}-1\right] \tag{13}$$

It depends on the values of the parameters α and β. For $\alpha \quad \beta \quad 0$ one has a pure damage process, with $\sigma_1' \to \sqrt{\frac{2E\zeta_0}{n_1}}$. After the tensile limit, the stress decreases as shown in the plot of Fig. 1(a) as does the elastic stiffness following the law $E(\omega_{1_e}) = E(1+\omega_{1_e})^{n_1}$. In Graph 1(b) the lateral deformation is reported. Given the form chosen for the fracture-like criterion, it was assumed that in tension tests the elastic limit coincides with the peak one.

The area E_f below the uniaxial curve is proportional to the fracture energy divided by a characteristic length, of the order of the diameter of the largest aggregate. In the present model the expression of the fracture energy E_f is given by the sum of two contributions:

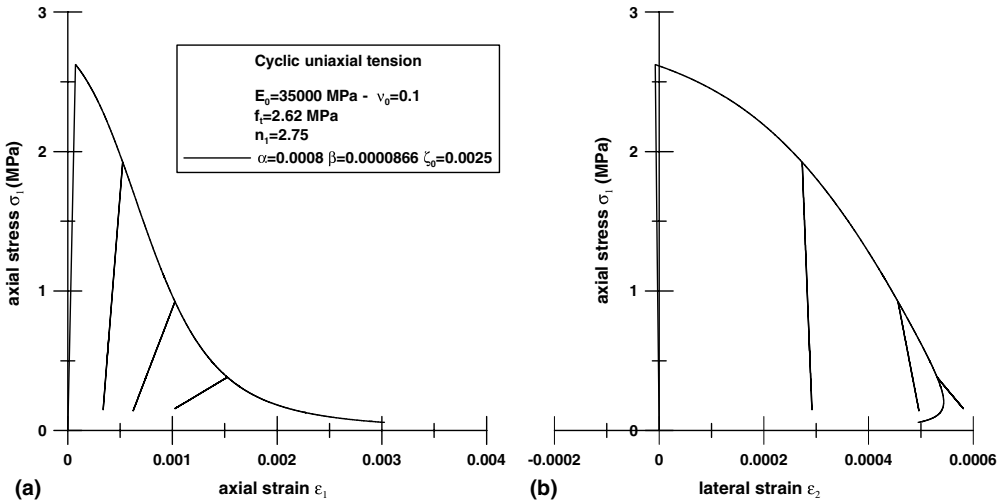

Fig. 1. Uniaxial cyclic tensile process. (a) Axial strain vs. axial stress. (b) Lateral strain vs. axial stress.

$$E_f = E_{f_1} + E_{f_2}$$

$$E_{f_1} = \frac{f_t^2}{2E_0} + \frac{n_1 - 1}{n_1}\zeta_0$$

$$E_{f_2} = \frac{G_0 K_0}{n_1^2(G_0 + 3K_0)}\left(\frac{q_3 q_4}{q_2} - \frac{3q_1}{q_2}\right)$$

$$q_1(\alpha,\beta) = 27\alpha^6 + 54\sqrt{3}\alpha^5\beta + 135\alpha^4\beta^2 + 60\sqrt{3}\alpha^3\beta^3 + +45\alpha^2\beta^4 + 6\sqrt{3}\alpha\beta^5 + \beta^6$$

$$q_2(\alpha,\beta) = (3\alpha^2 + 2\sqrt{3}\alpha\beta + \beta^2)^2$$

$$q_3(\alpha,\beta) = 81\alpha^7 + 189\sqrt{3}\alpha^6\beta + 567\alpha^5\beta^2 + 315\sqrt{3}\alpha^4\beta^3 + 315\alpha^3\beta^4 + 63\sqrt{3}\alpha^2\beta^5 + 21\alpha\beta^6 + \sqrt{3}\beta^7$$

$$q_4(\alpha,\beta) = \sqrt{9\alpha^2 + 6\sqrt{3}\alpha\beta + 3\beta^2 + \frac{2(G_0 + 3K_0)n_1\zeta_0}{G_0 K_0}}$$

It is possible to demonstrate the identity:

$$E_f = \zeta_0 \tag{14}$$

Fig. 2(a) presents the plot of the two terms of the fracture energy as a function of the damage exponent n_1. The relative weight of the two contributions changes with n_1 but their sum remains constant and equal to ζ_0. Therefore, the value of the constitutive parameter ζ_0 can be estimated from the fracture energy of the material.

The presence of coupling between damage and stress influences the shape of the limit envelope predicted by the criterion. Fig. 3 compares the biaxial limit envelope in the case $\alpha \quad \beta \quad 0$ (Fig. 3(a)), $\alpha \neq 0$, $\beta \quad 0$ (Fig. 3(b)), $\alpha \neq 0$, $\beta \neq 0$ (Fig. 3(c)).

The first form is not valid, since it is isotropic. In addition only the latter form with both the α and β parameters not equal to zero presents a corner point along the biaxial tensile axis, as it is observed in experimental failure envelopes. The latter has been used in the model.

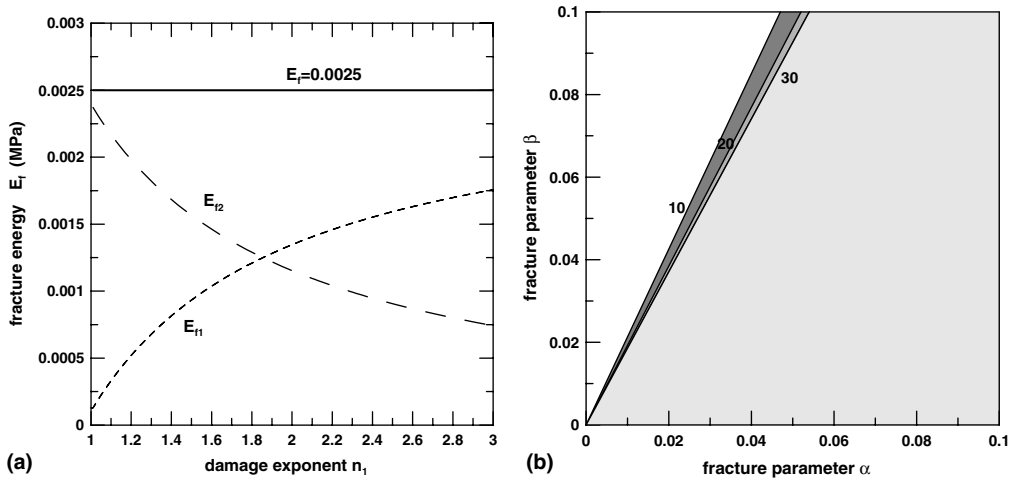

Fig. 2. (a) Fracture energy contributions. (b) Contour plot of the compressive tensile strength ratio.

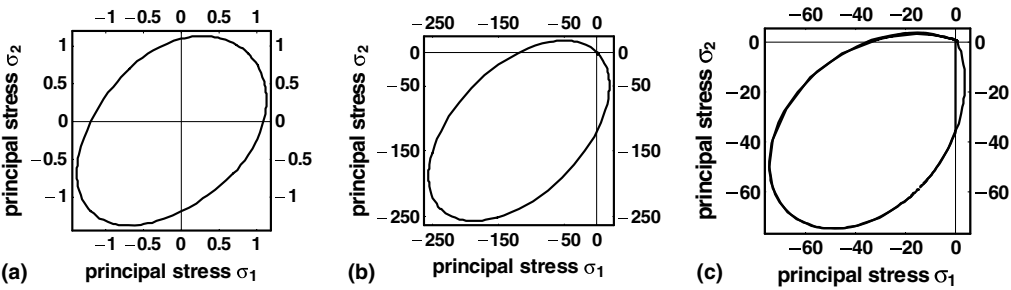

Fig. 3. Fracture criteria biaxial domains. (a) Pure damage fracture criterion $\alpha = \beta = 0$. (b) Fracture criterion $\alpha \neq 0$, $\beta = 0$. (c) Fracture criterion $\alpha \neq 0$, $\beta \neq 0$.

Therefore, the parameters α and β affect the shape of the limit envelope as well as the compression limit value of the strength predicted by the fracture criterion g_2. This limit, not applicable to normal concrete for which crashing occurs, can be effectively observed in highly compact rocks, such as marble or basalt, that collapse with abrupt explosions, so that no significant ductile deformation in compression is present. However, for these materials the ratio between compressive and tensile strength is quite large, of the order of 20 30, as predicted by criterion. Moreover, for some type of high strength concrete the compressive behavior can approach the one predicted by the criterion g_2.

Contour plots of the ratio between the compressive and the tensile limit stresses are reported in Fig. 2(b) as a function of the parameters α and β. The regions highlighted in the plot refer to ratios equal to 10, 20, 30, respectively. From this graph the pairs

(α, β) that guarantee the fulfillment of an assigned ratio and condition (13) can be estimated.

4.2. Compressive processes

In uniaxial compression the constitutive equations take the form:

$$\begin{aligned}
\sigma_1 &= \frac{9G_0K_0(1+\omega_{1_e})^{n_1}(1+\omega_{2_e})^{n_2}}{3K_0 + G_0(1+\omega_{1_e})^{n_1}(1+\omega_{2_e})^{n_2}}\varepsilon_{e_1},\\
\chi &= H[p_1(1+\omega_{1_e})^{n_1} + p_2(1+\omega_{2_e})^{n_2}]\alpha_e,\\
\zeta_1 &= \frac{n_1}{2}\frac{27G_0K_0^2(1+\omega_{1_e})^{n_1-1}(1+\omega_{2_e})^{n_2}}{[3K_0 + G_0(1+\omega_{1_e})^{n_1}(1+\omega_{2_e})^{n_2}]^2}\varepsilon_{e_1}^2,\\
\zeta_2 &= \frac{n_2}{2}\frac{27G_0K_0^2(1+\omega_{1_e})^{n_1}(1+\omega_{2_e})^{n_2-1}}{[3K_0 + G_0(1+\omega_{1_e})^{n_1}(1+\omega_{2_e})^{n_2}]^2}\varepsilon_{e_1}^2,\\
\nu^- &= \frac{3K_0 - 2G_0(1+\omega_{1_e})^{n_1}(1+\omega_{2_e})^{n_2}}{2[3K_0 + G_0(1+\omega_{1_e})^{n_1}(1+\omega_{2_e})^{n_2}]}.
\end{aligned} \tag{15}$$

Both the damage static variables evolve during the process. As will be shown in the next section, initially only the plastic criterion g_1 is activated and the variables ω_2 and α develop. However, since the damage forces ζ_1 keep increasing, the fracture criterion can also be activated, simulating the mixed form of the fracture pattern in the transition zone.

A numerical uniaxial compression test is presented in Fig. 4(a), where both the axial and the lateral strains are reported vs. the axial stress. The simulation is compared with experimental data from Imran and Pantazopoulou (1996) as elaborated by Park and Kim (2005); the predictions of the latter authors are also reported on the graph. The proposed model is able to simulate the initial non-linear damaging response, after the elastic limit has been reached, the attainment of the peak stress and the subsequent softening. In spite of the relative simplicity of our model with respect to competitive ones, it fits, with reasonable accuracy, either the axial or the lateral strain. A plot of the volumetric strain ε^v $\operatorname{tr}\varepsilon_e$ as a function of the axial strain is also shown in Fig. 4(b). The trend of the experimental data is reproduced, although using an associative plastic model.

The limit stress f_c appearing in the criterion g_1 refers to the elastic limit, usually quite difficult to detect experimentally and conventionally taken roughly equal to 30 40% of the peak stress. From the linear branches of the test it possible to estimate the initial elastic modulus E_0 and the Poisson ratio ν_0. The transition from the linear to the non-linear behavior is ruled by the initial hardening modulus H_0. In the experimental tests this transition is very smooth, so that in the model $H_0 = \frac{E_0E_{p0}}{E_0 - E_{p0}}$ should tend to infinity, E_{p_0} being the initial elasto-plastic modulus. However, an exceeding high value of H_0 would introduce severe numerical stability problems. Therefore a value near to 30 $50E_0$ has been used in the numerical simulations. The values of the damage parameters n_2 and k_ζ essentially affect the peak stress, the post-peak region, the amplitude of the area below the σ ε curve and the unloading modulus as well. They can be obtained by fitting uniaxial loading unloading tests. The same considerations hold true for the damage weight on the hardening p_1 and p_2. Lower values of p_2 and higher values of n_2 generate a less steep slope of the softening branch.

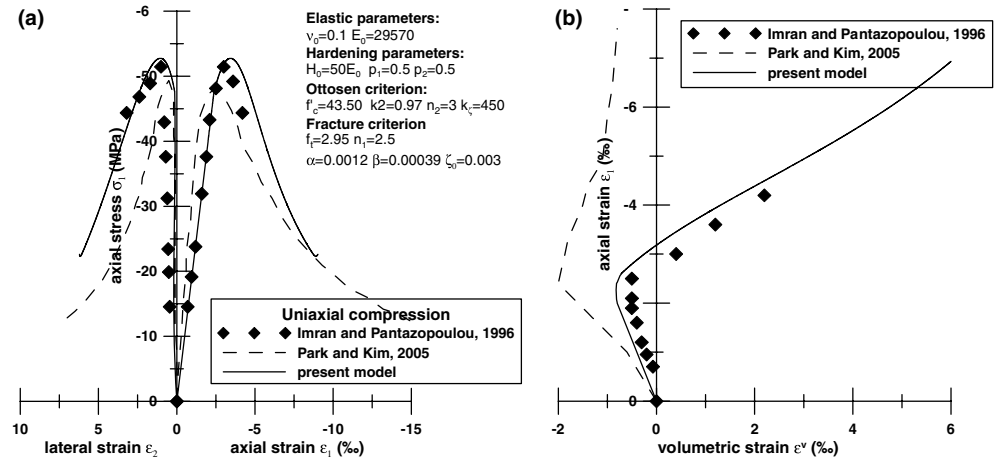

Fig. 4. Uniaxial compression. Comparison with Imran and Pantazopoulou (1996) experimental data. (a) Axial stress vs. axial and lateral strain. (b) Axial strain vs. volumetric strain.

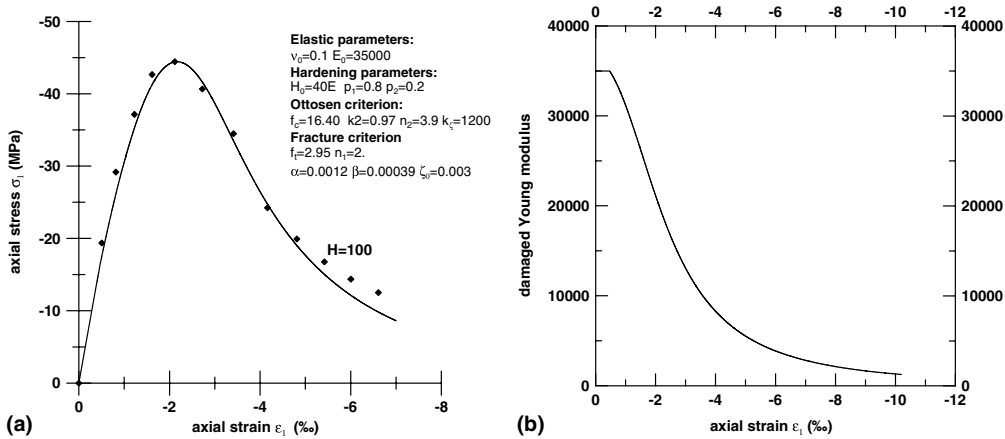

Fig. 5. Uniaxial compression. (a) Comparison with Mier (1984) experimental data. Axial stress vs. axial strain. (b) Damaged Young modulus.

A more severe comparison is presented in Fig. 5 with experimental data by Mier (1984) for prismatic specimens with eight H 100 mm. The test was carried up to strains larger than those commonly accepted in technical practice. The material parameters utilized in the simulation are indicated in the figure and have been obtained from the concrete properties reported in the original work. The fit is quite good for the axial strain (see Figs. 5(a) and (b) where the decay of the Young modulus is also shown) but it is rather poor for the lateral strain, even accounting for the large dispersion of the experimental data, as shown in Fig. 6.

It is well known that the post-peak curve is relative to localized deformations, so that its shape depends on the size of the specimen as has been shown, for instance, by the exper-

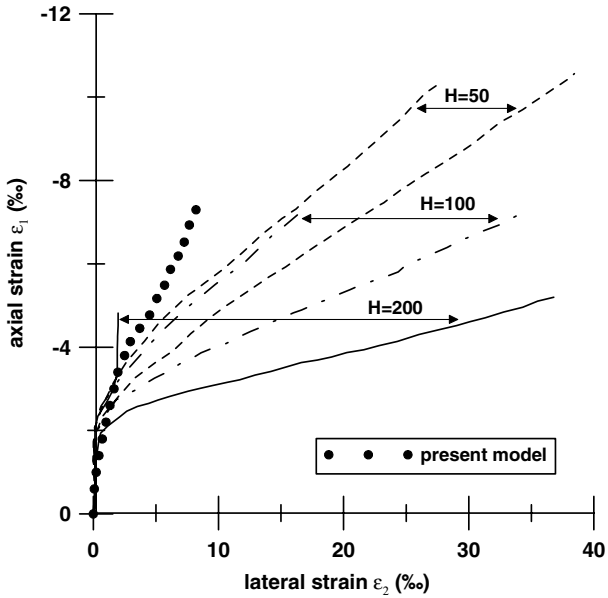

Fig. 6. Uniaxial compression. Comparison with Mier (1984) experimental data. Axial stress lateral strain curves. Influence of specimen height.

iments carried out by Mier (1984): a decreasing height of the specimen results in a decreasing slope in the stress strain curve descending branch, for a fixed cross-section, and in a lower dispersion of lateral strain measurements, as is shown in Fig. 6. No significant effect is evident, on the contrary, on the maximum stress. The experimental data should be delocalized, in order to be representative of the mechanical damage arising in a limited volume of the specimen (Bažant et al., 1996b)). The parameter κ_ζ that enters the model allows to a certain extent for delocalization, since it relates a localized damage to a damage variable defined per unit of volume. Indeed, the larger the value of κ_ζ, the sharper is the decay of the post-peak branch, as happens for high specimens. The necessity of some correction on the experimental data is one reason for the deviation in the numerical simulation of lateral strain from experimental data for high values of the axial strain. The main source of error, however, is probably due to the fact that the model is associated, i.e. no artificial dilatancy is introduced. In the following applications, however, the associative formulation is used, since it is a simplification for the convergence of the numerical algorithm and reasonably accurate within the technical range of interest.

The behavior of the model for the case of cyclic compression tension uniaxial test is analyzed in Fig. 7(a). The monotonic and cyclic cases are compared in order to underline that the peak stress, as well as the inelastic evolution of the deformation, are strongly path-dependent. The test has been performed between fixed strain limits, always unloading the specimen to zero deformation. Therefore, the trace of the elastic strain tensor is always negative, and no change in the slope of the unloading branches is observed.

On the contrary, performing the test of Fig. 7(b) where first a tensile strain is reached and then the strain is reversed to compression, it can be observed as the elastic slope changes between the tensile and the compressive range. In such a test, where severe tensile

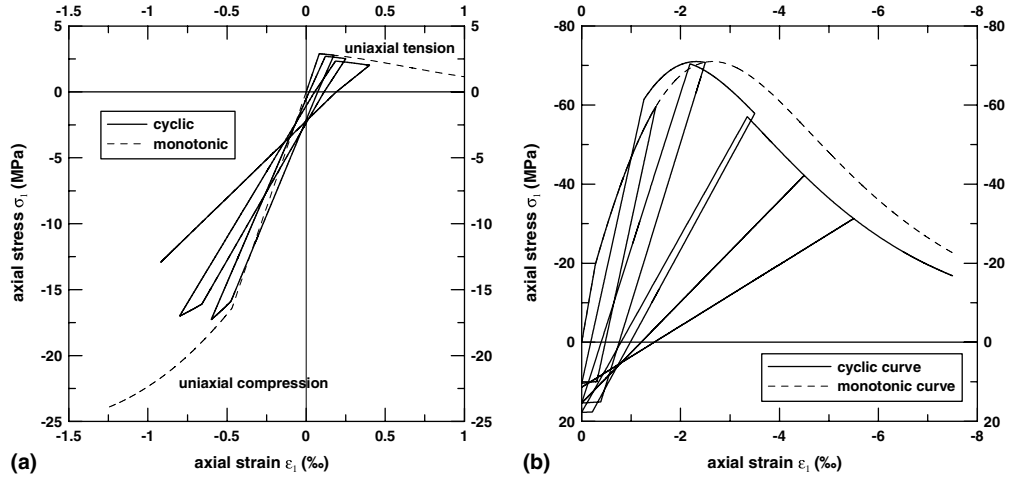

Fig. 7. (a) Uniaxial cyclic tension compression test. Degradation of the tangent modulus. (b) Uniaxial cyclic compression tension test. Comparison of monotonic and cyclic response.

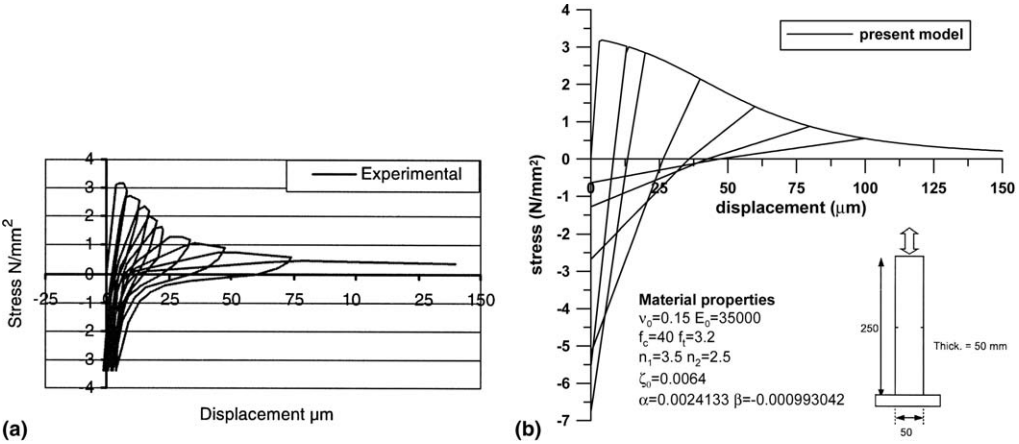

Fig. 8. Uniaxial cyclic tension test with crack opening and closing. (a) Reinhardt's experimental results. (b) Present model numerical results and Reinhardt's cyclic testing arrangement.

strains are reached, beyond the fracture limit, the stiffness of the material in compression rapidly decays.

A uniaxial loading unloading test on a notched specimen up to full crack closure at zero axial strain was carried out by Reinhardt (1984). Fig. 8(a) reports the experimental results, where the change of the tangent stiffness upon unloading can be clearly seen. It is quite well caught by the simulation, reported in Fig. 8(b) that was carried out at constitutive level only, i.e. the resistance of elastic area between the notches was not accounted for.

Confined compression tests are simulated in Fig. 9. First a hydrostatic pressure is applied, then the axial strain is increased up and beyond the peak stress. In the graph

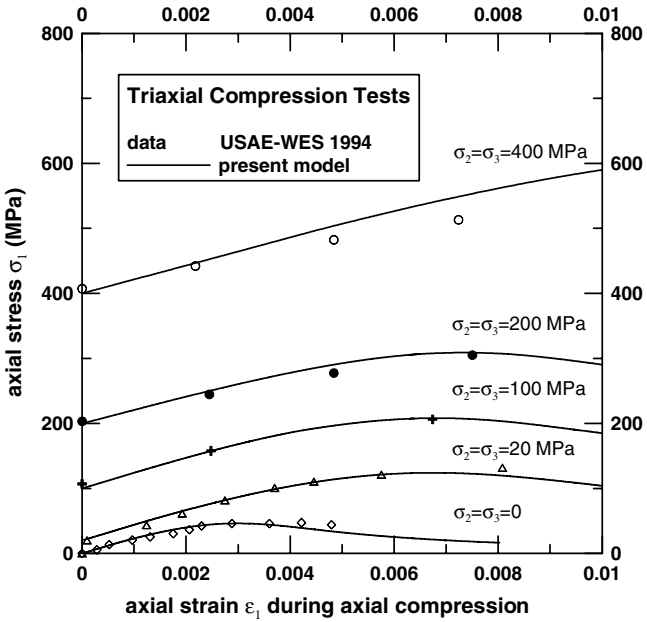

Fig. 9. Fitting of triaxial test data. Hydrostatic compression followed by uniaxial compression.

the axial stress takes the initial stress state into account, so at zero strain the curve departs from the value of the confinement pressure. At low levels of the confinement the behavior is distinctly softening and the peak stress is well-defined. Increasing the confinement pressure either the peak stress and the strain corresponding to the peak increase. For larger confinement ratios no peak stress can be detected. Therefore, the confinement implies an increase in the compressive strength and in the ductility of the material. In the numerical simulation the data of the uniaxial compression test in Fig. 9 and of the hydrostatic compression in Fig. 11(b) were used for calibrating the model.

4.3. Hydrostatic compression

Let's examine a process with $\varepsilon_{e_x} = \varepsilon_{e_y} = \varepsilon_{e_z} = \frac{\varepsilon_e^v}{3} < 0$. In the elastic regime, with $\omega_1 \quad \omega_2 \quad 0$, from (8) we have:

$$\begin{cases} \sigma_m & = K_0 \varepsilon_e^v \\ \chi^v & = 0 \end{cases}$$

K_0 being the undamaged bulk modulus. When the elastic limit hydrostatic stress is reached, i.e. $\sigma_m = \sigma_m^c$, the hydrostatic cap g_3 is activated and from the flow rule (10) we find:

$$\varepsilon_{p_x} = \varepsilon_{p_y} = \varepsilon_{p_z} = -\frac{\lambda}{3}$$

$$\alpha_p^v = -\lambda = \varepsilon_p^v = -\alpha_e^v$$

Therefore, in the post-elastic regime, it results:

$$\begin{cases} \sigma_m = K_0 \varepsilon_e^v = K_0(\varepsilon^v - \varepsilon_p^v) = K_0(\varepsilon^v + \lambda) \\ \chi^v = -\frac{D}{a} \ln \frac{a-\lambda}{a} \end{cases}$$

In this kind of loading condition the kinematic damage variables are constantly null, because only the cap g_3 is activated, that is no damage develops in hydrostatic compression. Furthermore, the damage forces ζ_1 and ζ_2 do not evolve during the entire process.

The yield condition becomes then:

$$-K_0(\varepsilon^v + \lambda) + \sigma_m^c + \frac{D}{a} \ln \frac{a-\lambda}{a} = 0 \tag{16}$$

Solving (16) for λ as a function of the imposed volumetric strain ε^v, it is possible to draw the plot of the hydrostatic stress σ_m vs. ε^v. A typical graph is shown in Fig. 10. The slope of the $\sigma_m - \varepsilon^v$ curve is given by:

$$\frac{\partial \sigma_m}{\partial \varepsilon^v} = K_0 \qquad \text{if } \lambda = 0, \ \ \varepsilon^v < \varepsilon_0^v$$

$$\frac{\partial \sigma_m}{\partial \varepsilon^v} = K_0 \left(1 + \frac{\partial \lambda}{\partial \varepsilon^v}\right) \qquad \text{if } \lambda \neq 0, \ \ \varepsilon^v > \varepsilon_0^v$$

From (16) we have

$$\varepsilon^v = \frac{1}{K_0} \left[\sigma_m^c + \frac{D}{a} \ln \frac{a-\lambda}{a} - K_0 \lambda\right]$$

so that:

$$\frac{\partial \varepsilon^v}{\partial \lambda} = -\frac{1}{K_0} \left[\frac{D}{a} \frac{1}{a-\lambda} + K_0\right]$$

$$\frac{\partial \sigma_m}{\partial \varepsilon^v} = K \frac{1}{1 + \frac{K_0}{D} a(a-\lambda)}$$

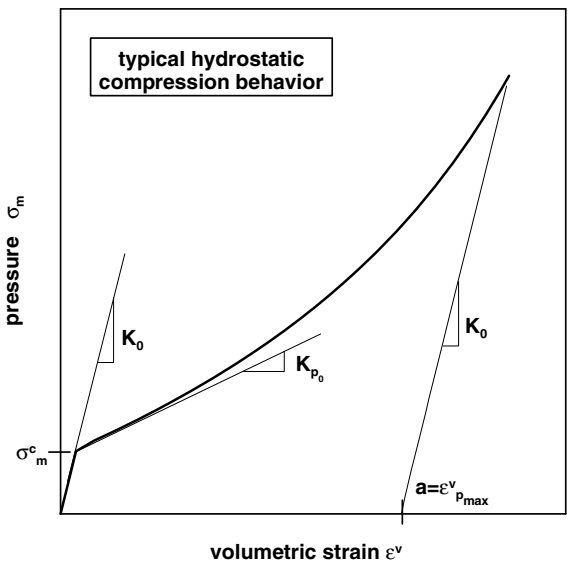

Fig. 10. Typical hydrostatic compression curve.

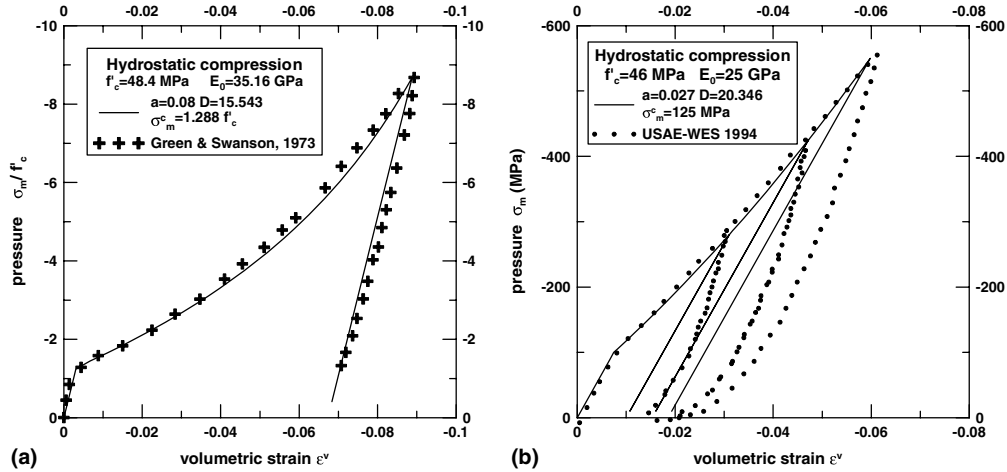

Fig. 11. (a) Fitting of hydrostatic compression test data by Green and Swanson (1973). (b) Fitting of hydrostatic compression data obtained at USAE. Waterways Experiment Station (1994).

The initial slope of the plastic region is given by:

$$K_{p_0} = \left.\frac{\partial \sigma_{\mathrm{m}}}{\partial \varepsilon^{\mathrm{v}}}\right|_{\lambda \to 0} = K_0 \frac{D}{D + Ka^2} \tag{17}$$

The value of K_{p_0} can be easily identified on the diagram of Fig. 10, as well as the σ^c_{m} limit stress. The maximum plastic volumetric strain $a = \varepsilon^{\mathrm{v}}_{p_{\max}}$ is reached when $\lambda \to a$ with slope equal to the elastic unloading:

$$\left.\frac{\partial \sigma_{\mathrm{m}}}{\partial \varepsilon^{\mathrm{v}}}\right|_{\lambda \to a} = K_0$$

Then the maximum void compaction a can be estimated reading on the $\sigma_m - \varepsilon^v$ graph of Fig. 10 the value of the residual volumetric strain corresponding to the point of the plastic branch with a slope near K_0. From (17) the estimation of the material parameter D is obtained:

$$D = \frac{K_0 K_{p_0}}{K_0 - K_{p_0}} a^2$$

Fig. 11(a) presents a comparison of the model prediction with the experimental hydrostatic compression test by Green and Swanson (1973). The agreement between the numerical and measured curves is good in both the loading and unloading branches. However, if a cyclic process is considered, despite the good reproduction of the envelope curve, the model is not able to predict hysteresis phenomena, as it is shown in the comparison of Fig. 11(b) with the experimental data obtained at the US Army Engineers Waterways Experiment Station (WES) in 1994 (Bažant et al., 1996b).

5. Multiaxial stress states and failure envelope

A numerical procedure has been used for calculating the evolution of the stresses up to the peak for several multiaxial load paths.

Any loading process is represented by a parametric curve in the extended space of stresses and conjugated forces. In the case of a virgin material the damage forces ζ_1 and ζ_2 evolve together with the stresses and their values have to be considered for the evaluation of the elastic limit state. The envelope of the elastic limit states, obtained by superposing the three criteria g_1, g_2, g_3, must therefore be evaluated for any particular loading path and depends on the values of the parameters of the three failure modes. Once the elastic limit is reached, the peak stress value can be evaluated only numerically and it is, as underlined in Section 4, path dependent.

The case of load paths defined by a fixed ratio between the stresses, i.e. radial paths, has been examined. Fig. 12 compares the elastic and the failure (peak) domain for biaxial stress states. The elastic domain is given by the intersection of the elastic generalized Ottosen domain and of the fracture domain, represented by the solid thin lines. The thickest solid line represent the failure envelope. The dotted line denotes the simple Ottosen damaged limit surface. Note the sharp difference between the elastic and the limit domain.

As mentioned in Section 4.2, in a uniaxial compression process first the Ottosen criterion is activated, but, due to the increase of both the damage variables, the fracture surface is reached, so that the peak stress in uniaxial compression is lower than the one obtained if only the plastic criterion is considered. On the contrary, in biaxial compression only plasticity is activated. In Fig. 12 the data by Mier (1984) have been used for parameter calibration.

Fig. 13 presents typical meridian sections of the elastic domain for the two values of the Lode angle $\vartheta = 0°$ and $\vartheta = 60°$, corresponding to the tensile and the compressive meridian respectively. The gap between the curves results in a marked triangular shape of the devi-

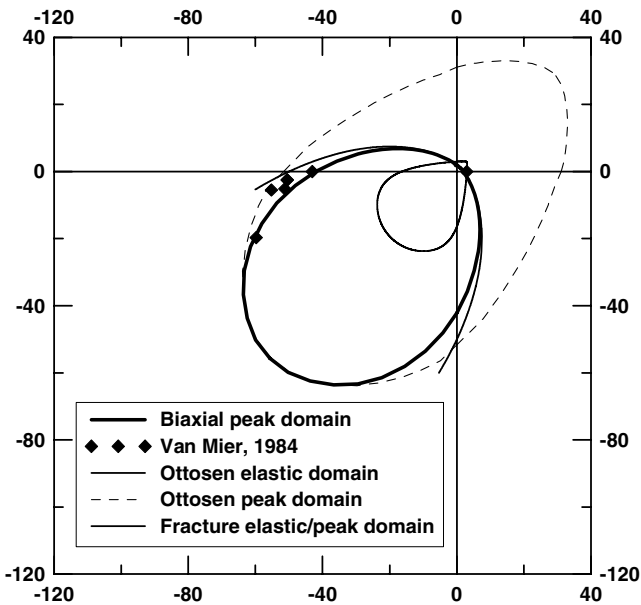

Fig. 12. Biaxial elastic and limit(peak) domain. Experimental data by Mier (1984).

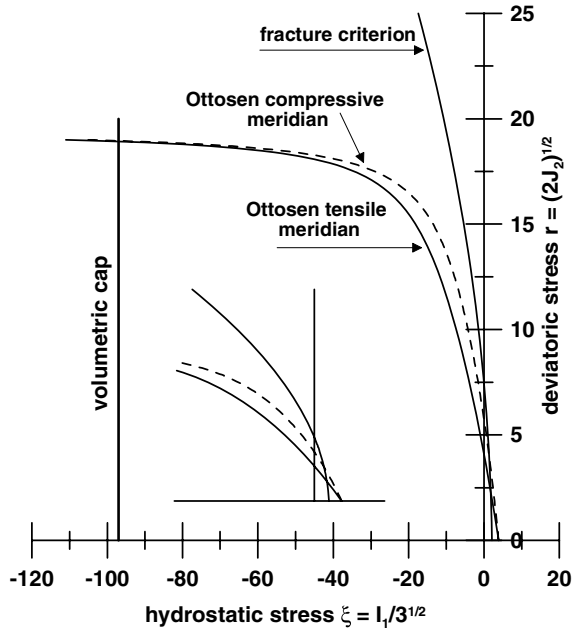

Fig. 13. Yield criteria on the meridian plane.

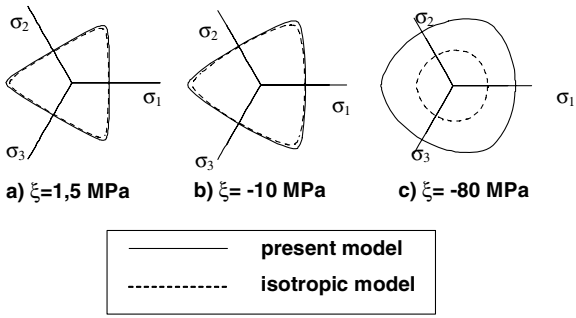

Fig. 14. Ottosen criterion: deviatoric sections for present model and isotropic model for different values of the hydrostatic stress.

atoric sections, as shown in Fig. 14. However, for large values of the confinement pressure, i.e. moving farther along the isotropic compression axis, the shape of the deviatoric sections gets more rounded, asymptotically tending to circular. In Fig. 14, a comparison with an isotropic damage model (Contrafatto and Cuomo, 2002) is also reported, showing that the present model predicts, according to experimental evidence, sharper deviatoric sections.

In Fig. 15(a) compression meridians (ϑ 60°) for elastic and limit envelopes are compared with the experimental results of triaxial tests by Mier (1984). The meridian sections present an asymptotic behavior for high values of the confinement pressure.

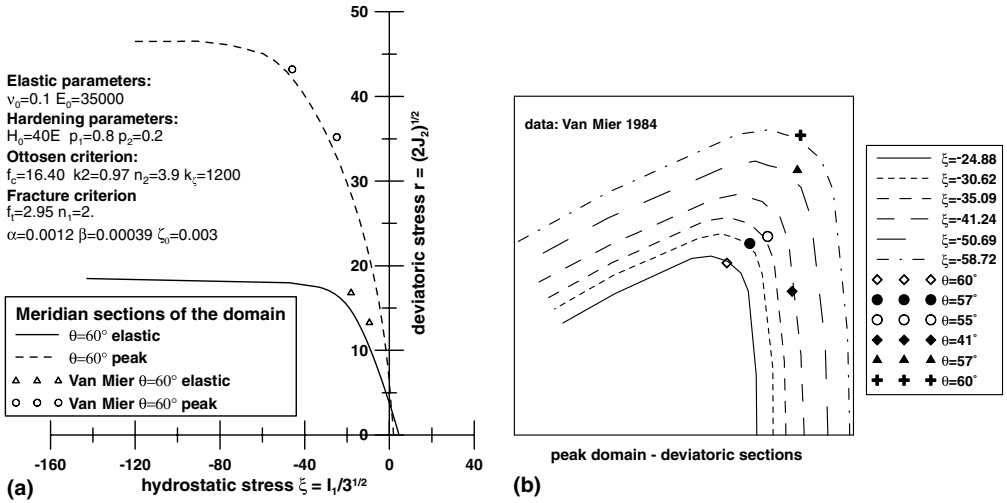

Fig. 15. Comparison with Mier (1984) experimental data. (a) Meridian section of the yield and peak domain. (b) Deviatoric sections of the failure envelope.

Fig. 15(b) shows the deviatoric sections of the failure domain for different values of the hydrostatic stress ξ; the dots report once again Van Mier experimental data. The agreement of the calculated peak stress with the experimental results is considerable for any value of the mean compressive stress ξ and of the Lode angle ϑ.

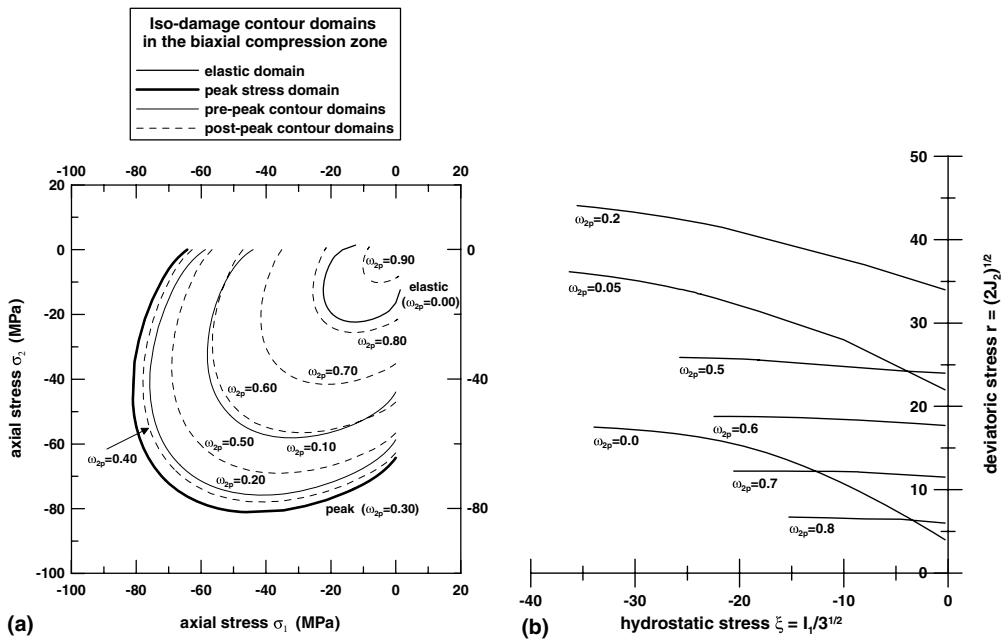

Fig. 16. Ottosen criterion. (a) Biaxial compression envelopes for fixed values of the damage variable ω_{2c}. (b) Iso damage compressive meridian sections.

One interesting feature of the model is the possibility of using the damage variables for structural control, defining serviceability limit states better than arbitrarily choosing deformation levels. In Fig. 16(a) iso-damage contour domains are reported for biaxial compression states. It is observed that the peak value is reached for the same damage level ($\omega_{2_p} \simeq 0.30$), independently of the stress ratio, so that the correspondent iso-damage contour domain coincides with the peak envelope. Further numerical investigations on different types of concrete and with different stress paths are needed to validate this result.

The evolution of the compression meridian with damage in the ξ r plane, obtained elaborating the numerical data of simulation of triaxial tests is represented in Fig. 16(b), showing how its slope, for values of the stress comparable to the uniaxial strength, decreases as damage progresses. This means that dilatancy decays from the initial value and tends to zero after the peak stress. This is in qualitative accordance with experimental findings and to an extent justifies the choice of an associative model.

6. Conclusions

The applications reported in Sections 4 and 5 suggest that following the methodology described in Section 3 some significant aspects of concrete mechanical behavior can be reproduced by a single elastic plastic-damage model. Simple and complex stress states have been simulated. The evolution of deformation and damage has been shown to be dependent on the load history as well as the peak stress and the energy dissipated after the peak. The implementation of the model is quite straightforward, being based on Continuum Damage Mechanics and an associative flow rule. This is a great advantage for the robustness of the numerical algorithm and for its use in structural codes for large 3D applications.

In the form presented in the paper the model has a certain number of limitations, some of which could easily be removed at the cost of greater complexity, as happens when a non associative plasticity is considered; other limitations are due to the uncertainties of the experimental data.

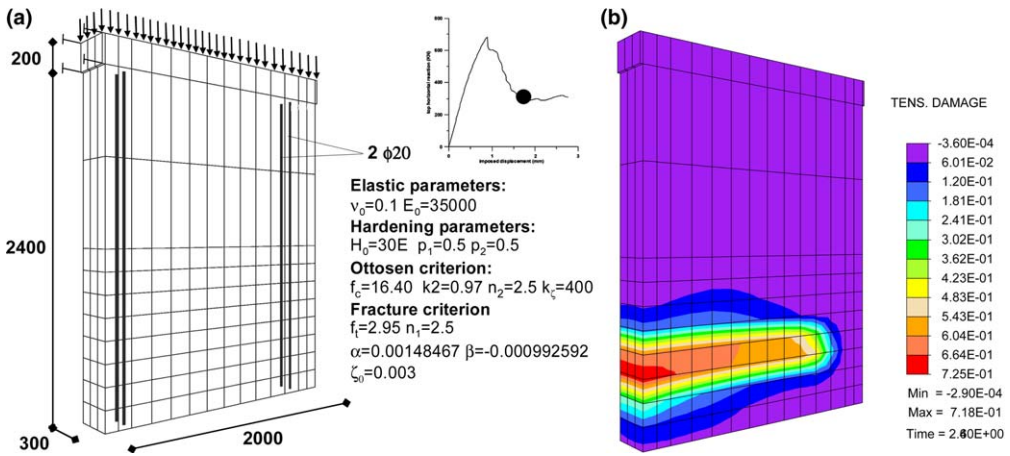

Fig. 17. Reinforced concrete wall. (a) Mesh, material data and loading condition. (b) Tensile damage distribution after the peak load.

In the model only isotropic damage has been considered for the sake of simplicity; in this way damage is spread over a finite zone and its directionality is accounted for by the evolution of the stress state. As an example, the behavior of a reinforced concrete wall, the top of which is subjected to constant compression and to an increasing horizontal displacement, has been investigated. The structure has been modelled with 3D elements. The tensile damage starts at the lower left corner, then, due to the confinement imposed by the built-in end of the wall, it migrates along the vertical edge and then progresses, as expected, following the horizontal direction, as shown in Fig. 17, where the geometry and the model parameters are also reported. A viscoplastic regularization was used for the simulation.

The extension of the model to anisotropic damage will be the subject of a subsequent paper. Other aspects of the model need better specification, like the form of the limit function for hydrostatic compression. Finally, a systematic optimization procedure should be developed for the parameter identification. Nevertheless, in the paper the main physical meaning of the various material parameters has been illustrated. Numerical issues, such as strain localization and computational procedures will be reported in a forthcoming paper that deals with applications to plain and reinforced concrete structure as well.

References

Bažant, Z., Di Luzio, G., 2004. Non local microplane model with strain softening yield limits. Int. J. Solids Struct. 41, 7209 7240.

Bažant, Z., Xiang, Y., Prat, P., 1996a. Microplane model for concrete. I: Stress strain boundaries and finite strain. J. Eng. Mech. (ASCE) 122 (3), 245 254.

Bažant, Z., Xiang, Y., Adley, M., Prat, P., Akers, S., 1996b. Microplane model for concrete. II: Data delocalization and verification. J. Eng. Mech. (ASCE) 122 (3), 255 262.

Bolzon, G., Fedele, R., Maier, G., 2002. Parameter identification of cohesive crack model by kalman filter. Comput. Methods Appl. Mech. Eng. 191, 2847 2871.

Brenchic, A., Gambarotta, L., 2001. Isotropic damage model with different tensile compressive response for brittle materials. Int. J. Solids Struct. 38, 5865 5892.

Carlson, D., Hoger, A., 1986. The derivative of a tensor valued function of a tensor. Quart. Appl. Math. 44, 409 423.

Carol, I., Jirásek, M., Bažant, Z., 2001. A thermodynamically consistent approach to microplane theory. Part I. Free energy and consistent microplane stresses. Int. J. Solids Struct. 38, 2921 2931.

Comi, C., Perego, U., 2001. Fracture energy based bi dissipative damage model for concrete. Int. J. Solids Struct. 38, 6427 6454.

Contrafatto, L., Cuomo, M., 2000. On a thermodynamically consistent continuum model for concrete coupled with quasi isotropic damage. In: Proceedings of the European Congress on Computational Methods in Applied Sciences and Engineering ECCOMAS 2000, Barcelona, Spain.

Contrafatto, L., Cuomo, M., 2002. A new thermodynamically consistent continuum model for hardening plasticity coupled with damage. Int. J. Solids Struct. 39, 6241 6271.

Contrafatto, L., Cuomo, M., 2005. A global convergent numerical algorithm for damaging elasto plasticity based on the multiplier method. Int. J. Numer. Methods Eng. 63, 1089 1125.

Curnier, A., He, Q. C., Zysset, P., 1993. Conewise linear elastic materials. J. Elasticity 37 (1), 1 38.

DiMaggio, F., Sandler, I., 1971. Material model for granular soils. J. Eng. Mech. Div. ASCE 97, 935 950.

Dragon, A., Halm, D., Désoyer, T., 2000. Anisotropic damage in quasi brittle solids: modelling, computational issues and applications. Comput. Methods Appl. Mech. Eng. 183, 331 352.

Faria, R., Oliver, J., Cervera, M., 1998. A strain based plastic viscous damage model for massive concrete structures. Int. J. Solids Struct. 35 (14), 1533 1558.

Frémond, M., Nedjar, B., 1995. Damage in concrete: the unilateral phenomenon. Nucl. Eng. Des. 156, 323 335.

Gambarotta, L., 2004. Friction damage coupled model for brittle materials. Eng. Fract. Mech. 71, 829 836.

Germain, P., 1973. Mécanique des Milieux Continues. Masson.
Green, S., Swanson, S., 1973. Static constitutive relations for concrete. Tech. Rep. AFWL TR 72 2, Air Force Weapons Lab., Kirtland Air Force Base, Albuquerque, N.M.
Halphen, B., Nguyen, Q., 1975. Sur les matériaux standards généralisés. J. Mecanique 14, 39 63.
Hansen, N., Schreyer, H., 1994. A thermodynamically consistent framework for theories of elastoplasticity coupled with damage. Int. J. Solids Struct. 31 (3), 359 389.
Imran, I., Pantazopoulou, S., 1996. Experimental study of plain concrete under triaxial stress. ACI Mater. J. 93 (6), 589 601.
Jefferson, A., 2003. Craft a plastic damage contact model for concrete. I. Model theory and thermodynamic considerations. Int. J. Solids Struct. 40, 5973 5999.
Jirásek, M., Zimmermann, T., 1998. Rotating crack model with transition to scalar damage. J. Eng. Mech. 124 (3), 277 284.
Klisinski, M., Mróz, Z., 1988. Description of inelastic deformation and degradation of concrete. Int. J. Solids Struct. 24 (4), 391 416.
Kuna Ciskał, H., Skrzypek, J., 2004. CDM based modelling of damage and fracture mechanisms in concrete under tension and compression. Eng. Fract. Mech. 71, 681 698.
Kupfer, H., Gerstle, K., 1973. Behavior of concrete under biaxial stresses. J. Eng. Mech. Div. (ASCE) 99, 853 866.
Litewka, A., Debinski, J., 2003. Load induced oriented damage and anisotropy of rock like materials. Int. J. Plasticity 19, 2171 2191.
Lu, P., Li, Q., Song, Y., 2004. Damage constitutive of concrete under uniaxial alternate tension compression fatigue loading based on double bounding surfaces. Int. J. Solids Struct. 41, 3151 3166.
Lubarda, V., Krajcinovic, D., Mastlovic, S., 1994. Damage model for brittle elastic solids with unequal tensile and compressive strenghts. Eng. Fract. Mech. 49, 681 697.
Lubliner, J., Oliver, J., Oller, S., Onate, E., 1989. A plastic damage model for concrete. Int. J. Solids Struct. 25 (3), 299 326.
Luccioni, B., Oller, S., Danesi, R., 1996. Coupled plastic damage model. Comput. Methods Appl. Mech. Eng. 129, 81 89.
Marfia, S., Rinaldi, Z., Sacco, E., 2004. Softening behavior of reinforced concrete beams under cyclic loading. Int. J. Solids Struct. 41, 3293 3316.
Mazars, J., 1986. A description of micro and macroscale damage of concrete structures. Eng. Fract. Mech. 25 (5/6), 729 737.
Mosler, J., Bruhns, O., 2004. A 3D anisotropic elastoplastic damage model using discontinuos displacement fields. Int. J. Numer. Methods Eng. 60, 923 948.
Murakami, S., Kamiya, K., 1997. Constitutive and damage evolution equations of elasti brittle materials based on irreversible thermodynamics. Int. J. Mech. Sci. 39 (4), 473 486.
Ortiz, M., 1985. A constitutive theory for the inelastic behavior of concrete. Mech. Mater. 4 (1), 67 93.
Ottosen, N., 1977. A failure criterion for concrete. J. Eng. Mech. Divi. (ASCE) 103 (4), 527 535.
Papa, E., Taliercio, A., 1996. Anisotropic damage model for the multiaxial static and fatigue behaviour of plain concrete. Eng. Fract. Mech. 55 (2), 163 179.
Papadopulos, P., Lu, J., 2001. On the formulation and numerical solution of problems in anisotropic finite plasticity. Comput. Methods Appl. Mech. Eng. 190, 4889 4910.
Park, H., Kim, J., 2005. Plasticity model using multiple criteria for concrete in compression. Int. J. Solids Struct. 42, 2303 2322.
Pietruszczak, S., Jiang, J., Mirza, F., 1988. An elastoplastic constitutive model for concrete. Int. J. Solids Struct. 24 (7), 705 722.
Reinhardt, H., 1984. Fracture mechanics of an elastic softening material like concrete. Heron 29 (2), 1 42.
Resende, L., 1987. A damage mechanics constitutive theory for the inelastic behaviour of concrete. Comput. Meth. Appl. Mech. Eng. 60, 57 93.
Salari, M., Saeb, S., Willam, K., Patchet, S., Carrasco, R., 2004. A coupled elastoplastic damage model for geomaterials. Comput. Methods Appl. Mech. Eng. 193, 2625 2643.
Sellier, A., Bary, B., 2002. Coupled damage tensors and weakest link theory for the description of crack induced anisotropy in concrete. Eng. Fract. Mech. 69, 1925 1939.
Sfer, D., Carol, I., Gettu, R., Etse, G., 2002. Study of the behaviour of concrete under triaxial compression. J. Eng. Mech. (ASCE) 128 (2), 156 163.

Taylor, R., 2002. FEAP – A Finite Element Analysis Program. University of California at Berkeley, Berkeley, CA.

Van Mier, J., 1984. Strain softening of concrete under multiaxial loading conditions. Ph.D. Thesis, Technische Wetenschappen aan de Technische Hogeschool, Eindhoven.